

Effect of nonlinear tide-surge interaction in the Pearl River Estuary during Typhoon Nida (2016)

Linxu Huang^{1,2}, Tianyu Zhang^{2,3,4}, Shouwen Zhang^{2*}, Hui Wang^{1,5}

1. Institute of Marine Science and Technology, Shandong University, Qingdao 266237, China

2. Southern Marine Science and Engineering Guangdong Laboratory (Zhuhai), Zhuhai 519082, China

3. Laboratory for Coastal Ocean Variation and Disaster Prediction, College of Ocean and Meteorology, Guangdong Ocean University, Zhanjiang 524088, China

4. Key Laboratory of Climate, Resources and Environment in Continental Shelf Sea and Deep Sea of Department of Education of Guangdong Province, Guangdong Ocean University, Zhanjiang 524088, China

5. National Marine Environmental Forecasting Center, Beijing 100086, China

*zhangshouwen@sml-zhuhai.cn

Abstract

Storm surge is one of the most significant marine dynamic disasters affecting the coastal areas worldwide. A comprehensive study of its mechanisms is vital for improving forecasting capabilities and developing more prevention strategies. In this study, a two-dimensional (2D) numerical model based on the Advanced Circulation Model (ADCIRC) was employed to examine the characteristics of storm surges and the mechanisms of tide-surge interaction in the Pearl River Estuary (PRE) during Typhoon Nida (2016). Three distinct model runs were conducted to differentiate between variations in water levels attributable to astronomical tides, storm surges, and their combined effect. The results indicated that storm tide are primarily modulated by tides through tide-surge interactions. The nonlinear effect of tide-surge interaction is primarily generated by the nonlinear local acceleration term and convection term from the tide-surge interactions in the study area, as derived from the mathematical terms. However, in regions of shallow water, such as the northern part of Qi'ao Island and Shenzhen Bay, they are predominantly governed by the nonlinear wind stress term and bottom friction term. Furthermore, the variations in the y component of the nonlinear momentum terms are more significant than those in the x component. To investigate the impact of tidal phase on storm surge response to Typhoon Nida, the timing of landfall was altered in order to introduce variations in PRE characteristics. The results demonstrate that the contribution ratio of each nonlinear term remains relatively constant, while the magnitudes exhibit fluctuations contingent on the timing of landfall.

Keywords: Tide-surge interaction; Storm surge; ADCIRC; Nonlinear effect

1. Introduction

Storm surges are defined as an abnormal rise in sea level caused by atmospheric pressure and wind stress from phenomena such as tropical cyclones (TCs) and fronts. TCs, also known as typhoons or hurricanes, have the potential to induce storm surges with extreme water levels, which can resulting in significant economic losses and human casualties in coastal areas, particularly when they coincide with high astronomical tides (Flather, 1994). The conventional method for forecasting storm surges during TCs involves predicting the water level under a specified wind

删除[Linxu Huang]: n in-depth

删除[Linxu Huang]: crucial

删除[Linxu Huang]: skills

删除[Linxu Huang]: implementing

删除[Linxu Huang]: better prevention measures

删除[Linxu Huang]: used

删除[Linxu Huang]: investigate

删除[Linxu Huang]: different

删除[Linxu Huang]: types of

删除[Linxu Huang]: distinguish

删除[Linxu Huang]: variations caused by

删除[Linxu Huang]: tide-surge interactions

删除[Linxu Huang]: surges

删除[Linxu Huang]: mainly

删除[Linxu Huang]: .

删除[Linxu Huang]: in shallow water regions such as th...

删除[Linxu Huang]: Additionally

删除[Linxu Huang]: we altered the

删除[Linxu Huang]: timing

删除[Linxu Huang]: shows

删除[Linxu Huang]: changes little

删除[Linxu Huang]: their

删除[Linxu Huang]: fluctuate

删除[Linxu Huang]: depending

删除[Linxu Huang]: s

删除[Linxu Huang]: ,

删除[Linxu Huang]: can

删除[Linxu Huang]: that

删除[Linxu Huang]: result

删除[Linxu Huang]: severe

删除[Linxu Huang]: especially

删除[Linxu Huang]: typhoon

field and then linearly add that water level to the predicted astronomical tides (Heaps, 1983). However, numerous studies have demonstrated that the effect of tide-surge interaction is nonlinear (Johns et al., 1985; Bernier and Thompson, 2007; Quinn et al., 2012). A comparison of observations with the straightforward linear superposition of astronomical tides and individually calculated storm surges indicates that discrepancies of up to 1-2 m (Rego and Li, 2010).

It is widely known that the total water level can be divided into three main components: the astronomical tide, the storm surge caused by atmospheric forcing, and the nonlinear residual level caused by tide-surge interaction which represents a significant source of error in the prediction of storm surges (Idier et al., 2012; Xu et al., 2016; Yang et al., 2019). Observations and simulations have indicated that storm surges are influenced by astronomical tides, with the nonlinear effect of the tide-surge interaction can significantly modulate water levels in shallow regions. There are two main characteristics of storm surges due to the nonlinear effect of tide-surge interaction. One characteristic is that the peak storm surge height near high tide is typically lower than that near low tide, which could increase storm surge levels during the rising tide and decrease them at high tide (Rossiter, 1961; Wolf, 1978; Horsburgh and Wilson, 2007; Olbert et al., 2013). Another characteristic is the variation in storm surge intensity, where the storm surge is notably stronger during low tide compared to high tide (Horsburgh and Wilson, 2007; Feng et al., 2016; Song et al., 2020). The tide-surge interaction comprises three nonlinear physical processes: (a) the nonlinear advective effect from the advective terms in the momentum equations; (b) the nonlinear bottom friction effect with quadratic parameterization; (c) the shallow water effect arising from the nonlinear terms related to the total water depth in both the mass conservation equation and the momentum equations (Zhang et al., 2010; Song et al., 2020; Zheng et al., 2020). Zhang et al. (2010) found that bottom friction was the principal contributor to tide-surge interaction in the Taiwan Strait. Rego and Li (2010) studied the storm surge induced by Hurricane Rita and revealed that the advection terms were dominant over bottom friction with significant spatial-temporal variations in the nonlinear terms. In strong current regions, the nonlinear advection term may also play a key role in the dynamics of nonlinear tide-surge interactions (Wolf, 1978; Rego and Li, 2010; Yang et al., 2019; Hu et al., 2023). Valle - Levinson et al. (2013) found that Coriolis accelerations and local accelerations due to alongshore current may significantly influence the tidal modulation of storm surges.

The characteristics of storm surges and nonlinear effects in the Pearl River Estuary (PRE) are especially complex, as its topography consists of deep channels, shallow shoals, and tidal flats. This renders the PRE highly susceptible to storm surges induced by intense TCs (Zheng et al., 2020). As a semi-enclosed bay, as shown in Fig 1c, Lingding Bay is regularly affected by both storm surges and irregular semi-diurnal tides. The trumpet-shaped bay naturally funnels tidal energy, leading to an amplification of tidal amplitude of at the top of the bay. However, specific investigations concerning the variability of typhoon landfall timing to tide-surge interactions and their impact on the temporal and spatial distribution of storm surges within the PRE are still scarce. Due to the strong tidal dynamics and complex topography in the region, tide-surge interactions along the PRE are significant, and the mechanisms are complex, which motivates this work. Therefore, efficient and accurate marine forecasting, achieved through the analysis of mechanisms and precise modeling of storm surges induced by typhoons, are essential for mitigating typhoon-induced disasters in coastal regions.

The maximum storm surge induced by Typhoon Nida, which coincided with the astronomical

删除[Linxu Huang]: Compared

删除[Linxu Huang]: with

删除[Linxu Huang]: ,

删除[Linxu Huang]: simple

删除[Linxu Huang]: separately

删除[Linxu Huang]: can lead to errors

删除[Linxu Huang]: pure

删除[Linxu Huang]: is

删除[Linxu Huang]: prediction

删除[Linxu Huang]: and

删除[Linxu Huang]: nonlinear

删除[Linxu Huang]: especially complex,

删除[Linxu Huang]: as the PRE is one of the most important economic regions of China. The topography of the PRE consists of

删除[Linxu Huang]: ,

删除[Linxu Huang]: which

删除[Linxu Huang]: makes

删除[Linxu Huang]: extremely

删除[Linxu Huang]: vulnerable

删除[Linxu Huang]: strong

删除[Linxu Huang]: Besides, it is a typical area with

删除[Linxu Huang]: ,

删除[Linxu Huang]: complicating tide-surge interactions.

删除[Linxu Huang]: accurate

删除[Linxu Huang]: is

85 | ~~high tide, resulted in severe economic losses, estimated at 19 million dollars.~~ The ~~principal~~
86 | ~~objective~~ of this study ~~is~~ to investigate the nonlinear residual levels associated with tide-surge
87 | ~~interactions caused by Typhoon Nida.~~ Additionally, ~~the objective is to investigate~~ the dynamic
88 | mechanisms by establishing mathematical relationships between these nonlinear levels and the
89 | nonlinear dynamic terms. In this paper, we utilize a recently developed ADCIRC based PRE surge
90 | model, which is nested within the China Sea tide and surge model, to investigate the mechanism
91 | of tide-surge interaction. In order to better characterize these impacts, different contributions to
92 | storm surge events can be calculated separately using nonlinear terms of the two-dimensional
93 | theoretical momentum equations (Yang et al., 2019; Song et al., 2020; Hu et al., 2023).

94 | In this paper, we will outline the characteristics of Typhoon Nida and provide a detailed
95 | description of the coupled tide-surge model, which is introduced and validated in Section 2. This
96 | is followed by an examination of the distribution of storm surge levels and nonlinear levels, along
97 | with a discussion of the results in Section 3. The conclusions derived from this study are detailed
98 | in Section 4.

99 |

删除[Linxu Huang]: main
删除[Linxu Huang]: s
删除[Linxu Huang]: are
删除[Linxu Huang]: , which coincided with the astronomical
high tide in the PRE
删除[Linxu Huang]: we aim to explore

100 | 2. Materials and Method

101 | In this study, a coupled tide-surge model was built for Typhoon Nida. The typhoon and
102 | associated numerical model are introduced, and the model setup and validations are also
103 | described.

104 | 2.1 Typhoon ~~Nida~~

105 | Typhoon Nida ~~was~~ generated in the western North Pacific Ocean on 29 July 2016, and
106 | ~~subsequently~~ began to move westward rapidly. As shown in Fig 1a, ~~it as a sever tropical storm~~
107 | ~~(STS).~~ Typhoon Nida passed across the Philippines and entered the South China Sea (SCS) on
108 | July 31, 2016. It ~~continued~~ westward and made landfall ~~as a typhoon (TY)~~ at 19:30 on August 1 in
109 | Shenzhen, Guangdong Province, China. ~~Typhoon Nida~~ had a central pressure of 970 hPa and
110 | maximum wind speed exceeding 42 m/s. ~~After that, it weakened into a tropical storm (TS). At~~
111 | ~~0:00 on August 3, it further weakened into a tropical depression (TD) before dissipating. Notably,~~
112 | the peak ~~water level~~ increase caused by ~~the storm surge of~~ Typhoon Nida coincided with the
113 | ~~highest~~ high water (HHW) tidal phase. ▼

设置格式[Linxu Huang]: 字体: 小四, 加粗
删除[Linxu Huang]: **NIDA**
设置格式[Linxu Huang]: 字体: 小四, 加粗
删除[Linxu Huang]: then proceeded
删除[Linxu Huang]: The typhoon
删除[Linxu Huang]: It
删除[Linxu Huang]: is significant that
删除[Linxu Huang]: surge-induced
删除[Linxu Huang]: higher
删除[Linxu Huang]: Typhoon Nida caused severe economic
loss, with an estimated impact of 19 million dollars.

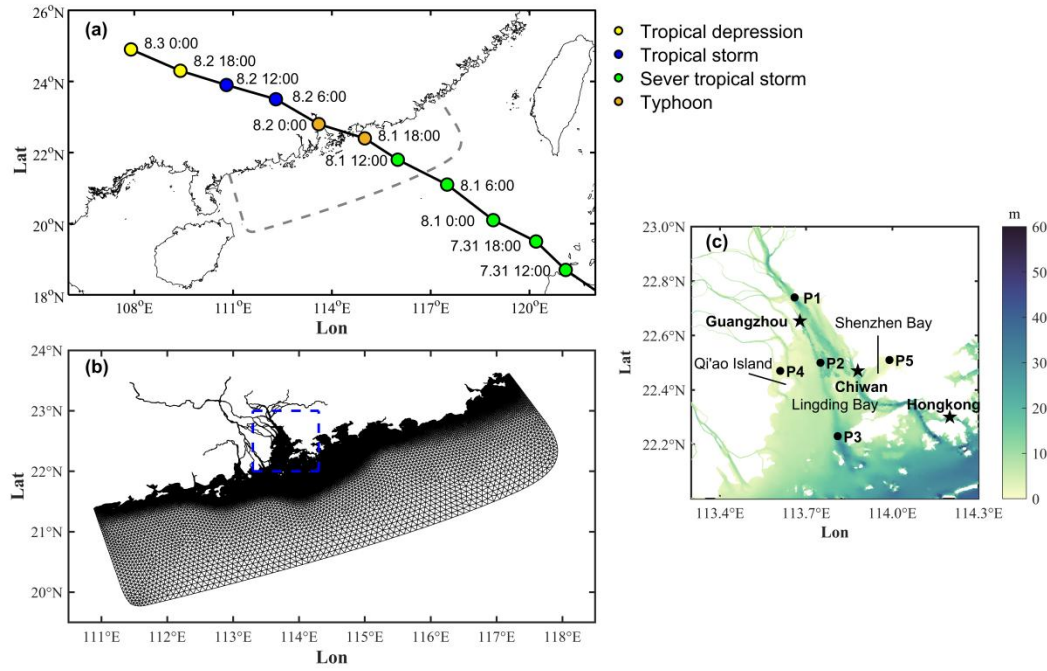


Figure 1. (a) The track and intensity of Typhoon Nida; (b) Model domain and grids of the study area; (c) Location and bathymetry of PRE. Stars represent the tidal gauges, and dots denote the calculation points of surge levels

2.2 The Numerical Model

The Advanced Circulation Model (ADCIRC) was used to simulate the tide and storm surge in PRE (Luettich et al., 1992). ADCIRC solves the primitive equations with the finite element method in space and with finite difference method in time (Westerink et al., 1992). Unstructured triangular grids were used in the horizontal plane to resolve dynamics in complex shorelines.

The basic vertically averaged governing equations, derived from momentum and continuity are as follows:

$$\begin{aligned} \frac{\partial H}{\partial t} + \frac{\partial}{\partial x}(UH) + \frac{\partial}{\partial y}(VH) &= 0 \\ \frac{\partial U}{\partial t} + U \frac{\partial}{\partial x}U + V \frac{\partial}{\partial y}U - fV &= -g \frac{\partial(\zeta + P_s / g\rho_0)}{\partial x} + \frac{\tau_{sx} - \tau_{bx}}{H\rho_0} - \frac{D_x}{H} \\ \frac{\partial V}{\partial t} + U \frac{\partial}{\partial x}V + V \frac{\partial}{\partial y}V + fU &= -g \frac{\partial(\zeta + P_s / g\rho_0)}{\partial y} + \frac{\tau_{sy} - \tau_{by}}{H\rho_0} - \frac{D_y}{H} \end{aligned} \quad (1)$$

Where (U, V) are the x and y depth-averaged velocity components; $H = h + \zeta$ is the total water level; ζ is free surface elevation; h is the water depth; f is the Coriolis force parameter; g is gravitational acceleration; P_s is sea surface atmospheric pressure; ρ_0 is sea water density; (τ_{sx}, τ_{sy}) are the x and y components of surface wind stress; (τ_{bx}, τ_{by}) are the x and y components of bottom friction; (D_x, D_y) are the horizontal momentum diffusion terms.

The surface wind stress parameters (τ_{sx}, τ_{sy}) are computed as follows:

$$\tau_{sx} = \rho_a C_d W_x \sqrt{W_x^2 + W_y^2}, \tau_{sy} = \rho_a C_d W_y \sqrt{W_x^2 + W_y^2} \quad (2)$$

Where ρ_a is air density; (W_x, W_y) are the x and y components of wind speed. C_d is the wind drag coefficient, from Garratt (1977), it is calculated as follows:

删除[Linxu Huang]:

设置格式[Linxu Huang]: 字体: 小四, 加粗

删除[Linxu Huang]: Which is unstructured

$$C_d = 0.001 \times (0.75 + 0.067 \sqrt{W_x^2 + W_y^2}) \quad (3)$$

The bottom friction (τ_{bx}, τ_{by}) is computed using the quadratic equation below:

$$\tau_{bx} = \rho_0 C_f U \sqrt{U^2 + V^2}, \tau_{by} = \rho_0 C_f V \sqrt{U^2 + V^2} \quad (4)$$

The bottom friction drag coefficient C_f is determined by model calibration.

The wind field model is crucial for accurate storm surge calculations. We employed the analytical wind model from Holland (1980), which was applied in reconstructing the wind field during Typhoon Nida. The radial distribution of wind and pressure are determined as follows:

删除[Linxu Huang]:
2.3 wind field of typhoon
删除[Linxu Huang]: has

$$P_s(r) = P_c + (P_n - P_c) \cdot \left(-\frac{R_{\max}}{r} \right)^B \quad (5)$$

$$W_g(r) = \sqrt{(P_n - P_c) \frac{B}{\rho_a} \left(\frac{R_{\max}}{r} \right)^B \exp\left(-\frac{R_{\max}}{r} \right)^B + \left(\frac{rf}{2} \right)^2 - \frac{rf}{2}} \quad (6)$$

Where r is the distance from the typhoon center; P_n is the ambient pressure (1010 hPa); P_c is the central pressure; R_{\max} is the maximum wind radius and W_g is wind speed. The B parameter determines the peak and intensity of the typhoon wind field, and is calculated as follows:

$$B = 1.5 + (980 - P_c) / 120 \quad (7)$$

As B increases, the strong wind becomes increasingly localized near the radius of maximum winds. For larger B , the wind drops off more abruptly both inside and outside the radius of maximum wind. The R_{\max} is calculated as follows:

$$R_{\max} = 51.6 \exp(-0.0223 V_{\max} + 0.0281 \varphi) \quad (8)$$

V_{\max} is the maximum wind and φ is latitude. The inflow angle caused by friction contributes to wind field asymmetry, and a constant angle of 25 is used in this paper. The central pressure and position data were retrieved from the China Meteorological Administration (CMA) tropical cyclone database (Lu et al., 2021).

2.3 Model setting

The grid resolutions were set at a maximum of 600 m at the open boundaries, while the finest resolution within the PRE region was 100 m. The domain space was discretized into 325582 triangular cells with 182048 nodes as shown in Fig 1b. The model utilized mean sea level as its reference datum, and was forced at the open boundaries by 8 tidal constituents (including M_2 , S_2 , N_2 , K_2 , K_1 , O_1 , P_1 and Q_1) derived from the global tidal model TPXO 9 (Egbert and Erofeeva, 2002). The typhoon wind field was generated using the wind model of Holland (1980). We used a two-dimensional (2D) hydrodynamic model based on ADCIRC for the simulation runs. The vertical current shear in well-mixed environment at shallow water depth is relatively small, therefore, the 2D depth averaged model is sufficient to reveal the physical processes of tide-surge interaction (Idier et al., 2012; Song et al., 2020; Zhang et al., 2017). The model was run with a cold start, setting both the current and water levels to zero at the initial time. The effect of river flow and wind-generated waves were not considered in our model simulation, as the research is primarily focused on the tide-surge interactions.

设置格式[Linxu Huang]: 字体: 小四, 加粗
删除[Linxu Huang]: 4
删除[Linxu Huang]: to 100 m
删除[Linxu Huang]: (
删除[Linxu Huang]:)

171 To verify the influence of the tide on storm surges, three simulations were conducted. One
172 was used to obtain the storm surge elevation (ζ_s) by only adding atmospheric forcing, another was
173 used to obtain the tide elevation (ζ_T) by only adding astronomical tidal forcing, and the other was
174 used to calculate the total water elevation (ζ_{TS}) by both atmospheric and tidal forcing. The storm
175 tide elevation (ζ_{TS}) can be written as the sum of the tide elevation (ζ_T), storm surge elevation (ζ_s),
176 and the nonlinear residual level (ζ_{Non}) due to tide-surge interaction, such that $\zeta_{TS} = \zeta_T + \zeta_s + \zeta_{Non}$.
177 Additionally, practical storm surge elevation $\zeta_{ps} = \zeta_{TS} - \zeta_T$ also considered in this paper.

179 3. Result

180 3.1 Tide and storm tide validation

181 The correlation coefficient (R), root mean square error ($RMSE$), model skill ($Skill$) were used
182 to validate the computed water level. The definition of the three indicators are determined as
183 follows:

184
$$Skill = 1 - \frac{\sum_{n=1}^N |M_n - C_n|^2}{\sum_{n=1}^N \left(|M_n - \overline{M_n}|^2 + |C_n - \overline{C_n}|^2 \right)} \quad (9)$$

185 Where M_n and C_n are the measurements and model computed results, respectively, at N
186 discrete point.

187 The computed astronomical tides were initially assessed at three hydrological stations,
188 Chiwan, Hong Kong, and Guangzhou, during the period from July 2 to July 30, 2016 (Fig 2). The
189 simulation results demonstrated a close match with the measurements obtained at these three
190 hydrological stations, as detailed in Table 1. The model predictions exhibited excellent agreement
191 with the reconstructed astronomical tide, with RMSE values at all three stations are < 0.27 m, both
192 the R values and Skill values are generally above 0.91.

193 The model simulated storm tide levels were further compared with the observed total water
194 levels at the aforementioned three stations, as depicted in Fig 3. At all three stations mentioned
195 above, the measured water level data reached its maximum (exceeding 2 m) on the evening of
196 August 1, shortly after Typhoon Nida made landfall. At the Chiwan station, the water level
197 exceeded 4 m, with a discrepancy of 0.21 m between the maximum of the simulated and the
198 measured data. At the Hong Kong station, there was a discrepancy of 0.13 m between the
199 maximum of the simulated and the measured data. At the Guangzhou station, there was a
200 discrepancy of 0.33 m between the maximum of the model, simulated storm tide and the measured
201 data. As illustrated in Table 1, the R value, RMSE value and the Skill value demonstrate that the
202 simulation is functioning effectively.

203 The numerical results shows that when Typhoon Nida approached to the PRE, the simulation
204 of increased water, was underestimated, resulting in significant errors in storm tide prediction.
205 However, the simulated results for maximum water levels were in close alignment with the
206 observed values, thereby demonstrating that the model used in this study is an effectively
207 representation of the tidal-surge interactions within the study area.

208

- 删除[Linxu Huang]: As a semi-enclosed bay, Lingdingya
- 删除[Linxu Huang]: carried out
- 删除[Linxu Huang]: pure
- 删除[Linxu Huang]: $T+S$
- 删除[Linxu Huang]:
- 删除[Linxu Huang]: 2.5
- 设置格式[Linxu Huang]: 字体: 小四, 加粗
- 删除[Linxu Huang]: surge
- 删除[Linxu Huang]:
$$R = \frac{\sum_{n=1}^N (M_n - \overline{M_n})(C_n - \overline{C_n})}{(N-1)\sigma_M \sigma_C}$$
- 删除[Linxu Huang]: 11
- 删除[Linxu Huang]:
- 设置格式[Linxu Huang]: 左, 缩进: 首行缩进: 7.4 毫米
- 删除[Linxu Huang]: -predicted
- 删除[Linxu Huang]: surge
- 删除[Linxu Huang]: peak
- 删除[Linxu Huang]: positive extreme value error
- 删除[Linxu Huang]: error of the positive extreme value
- 删除[Linxu Huang]: data
- 删除[Linxu Huang]: (Table 1)
- 删除[Linxu Huang]: And a
- 删除[Linxu Huang]: t
- 删除[Linxu Huang]: positive extreme value error
- 删除[Linxu Huang]: -predicted
- 删除[Linxu Huang]: negative surge levels are
- 删除[Linxu Huang]: overestimated
- 删除[Linxu Huang]: surge
- 删除[Linxu Huang]: positive surge
- 删除[Linxu Huang]: closely
- 删除[Linxu Huang]: match
- 删除[Linxu Huang]: represents

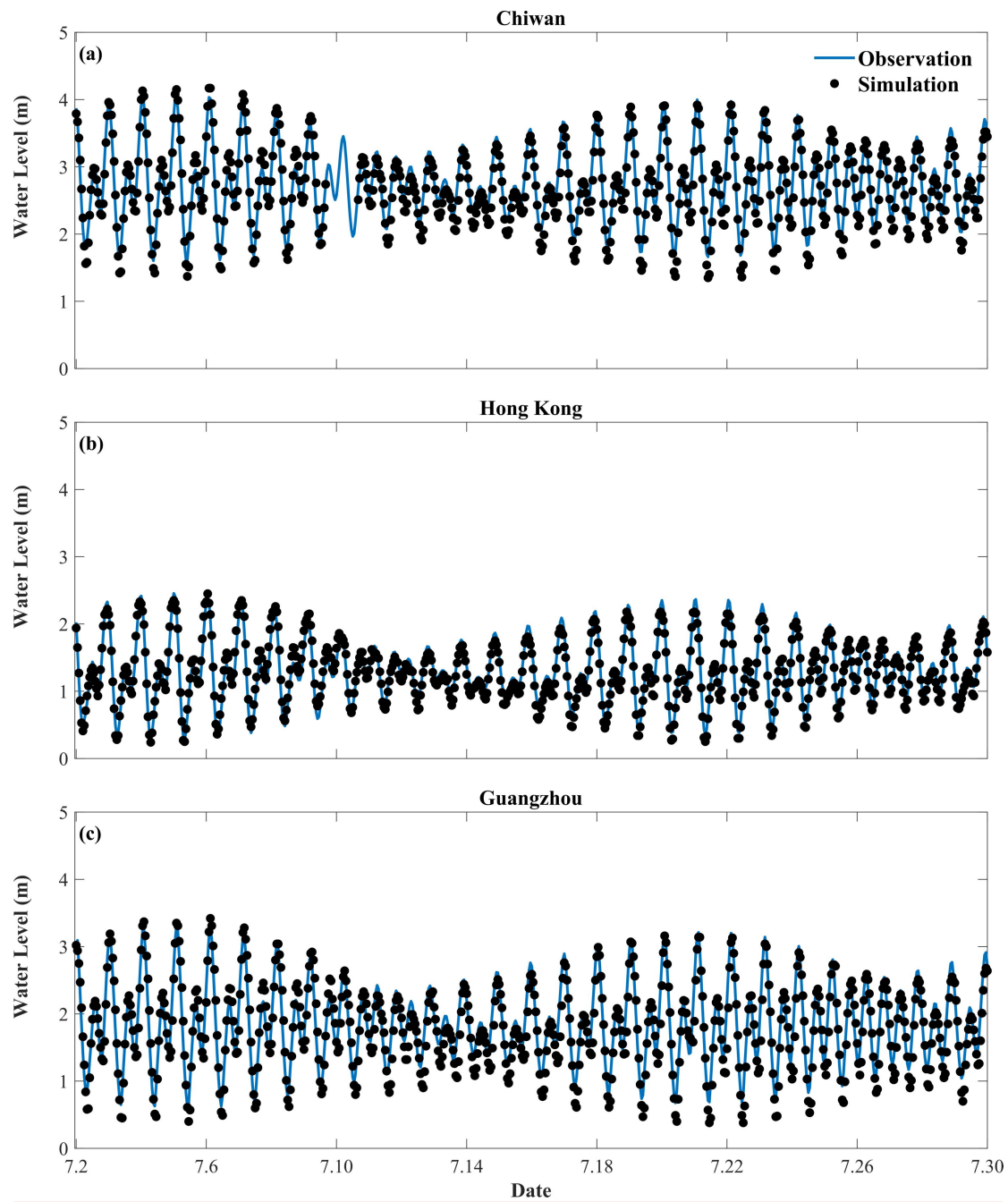


Figure 2. Time series comparisons of measured and modeled astronomical tide levels at (a) Chiwan gauge (b) Hongkong gauge (c) Guangzhou gauge

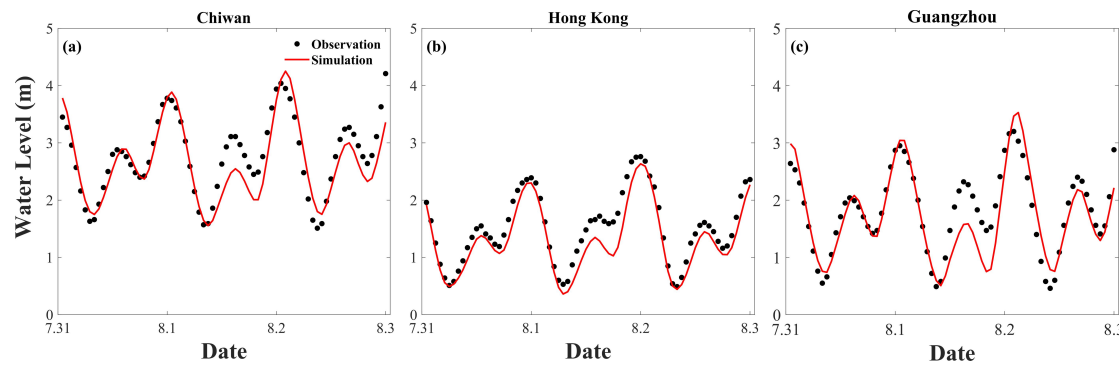


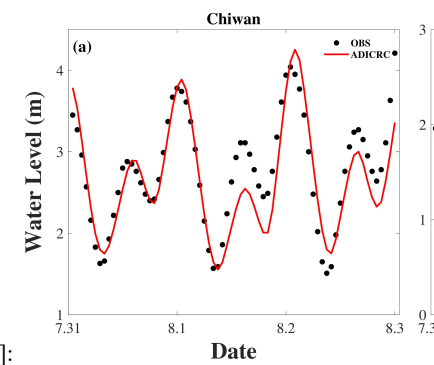
Figure 3. Time series comparisons of measured and modeled storm tide levels at (a) Chiwan gauge (b) Hong Kong gauge (c) Guangzhou gauge

Table 1. Comparisons of tide and storm tide between the model simulations and observations

Station		Chiwan	Hong Kong	Guangzhou
Tide	R	0.9470	0.9749	0.9206
	RMSE (m)	0.2046	0.1047	0.2629
	Skill	0.9368	0.9745	0.9112
Storm <u>tide</u>	R	0.9023	0.9728	0.8959
	RMSE (m)	0.3144	0.2503	0.3467
	Skill	0.8912	0.9169	0.8874

3.2 Storm surge characteristics of Typhoon Nida

Typhoon Nida passed through the PRE during a spring tide, coinciding with the maximum storm surge at the HHW tidal phase. Based on this phenomenon, five tidal phases were selected for investigate the evolution of storm surges before or after Typhoon Nida made landfall. The spatial and temporal distribution characteristics of storm tides elevation during various tidal phases in the PRE are illustrated in Fig 4. Five points were selected for examination within the internal (P1), middle (P2), external (P3), northern part of Qi’ao Island (P4), and Shenzhen Bay (P5) regions of the PRE, as shown in Fig 1c. Notably, the water depth at points P1, P2, and P3 exceeds 10 m, while the water depth at points P4 and P5 is less than 10 m. At 9:00 on 1 August, during the lowest low water (LLW) tidal phase, the PRE area showed a decreased in water elevation (Fig 4a), while the nonlinear residuals were positive in Shenzhen Bay and northern part of Qi’ao Island (Fig 4b). At 15:00 on 1 August, which coincides with the lowest high water (LHW) tidal phase, the storm tide elevation in PRE shows a negative to positive trend from northeast to southwest. The most notable decline in water elevation is observed in Shenzhen Bay (Fig 4d). At the same time, the nonlinear residuals are negative throughout Lingding Bay, with the exception of its upper region (Fig 4e). At 19:00 on 1 August, during the highest low water (HLW) tidal phase, a negative trend was observed in the elevation of storm tide in the PRE area, with the greatest negative values occurring from northeast to southwest. Notably, the greatest decrease in water elevation was observed in Shenzhen Bay, (Fig 4g). While the nonlinear residuals are positive, their impact is particularly significant in Shenzhen Bay and the northern part of Qi’ao Island (Fig 4h). During the HHW tidal phase, the storm tide elevation in the PRE area exhibits a most substantial increase (Fig 4j). Conversely, during the same phase, the nonlinear residuals exhibit a most significant decrease (Fig 4k). Furthermore, at 10:00 on 2 August, during the LLW tidal phase, the storm tide



删除[Linxu Huang]:

删除[Linxu Huang]: surge

删除[Linxu Huang]: surge

删除[Linxu Huang]: Surge

删除[Linxu Huang]: **3. Result**

删除[Linxu Huang]: **1**

删除[Linxu Huang]: positive

删除[Linxu Huang]: we

删除[Linxu Huang]: five tidal phases to

删除[Linxu Huang]: surges

删除[Linxu Huang]: at

删除[Linxu Huang]: different

删除[Linxu Huang]: are chosen

删除[Linxu Huang]: to examine this interaction,

删除[Linxu Huang]: 1st

删除[Linxu Huang]: lower

删除[Linxu Huang]: level

删除[Linxu Huang]: levels

删除[Linxu Huang]: 1st

删除[Linxu Huang]: ing

删除[Linxu Huang]: lowe

删除[Linxu Huang]: r

删除[Linxu Huang]: total water level

删除[Linxu Huang]: significant decrease

删除[Linxu Huang]: residual levels

删除[Linxu Huang]: shows that it is

删除[Linxu Huang]: in

删除[Linxu Huang]: yang

删除[Linxu Huang]: except

242 elevation in the PRE area was negative, while the nonlinear residuals are positive.

243 A comprehensive time series of storm surge elevation (ζ_s), tide elevation (ζ_T), storm tide

244 elevation (ζ_{TS}), practical storm surge elevation (ζ_{ps}) and nonlinear residuals (ζ_{Non}) for each of the

245 five points in the study area are also shown in Fig 4. The positive storm surge elevation at three

246 points (P1, P2, and P3) exhibited a notable increase, from the outer to the inner regions of

247 Lingding Bay. When Typhoon Nida made landfall, the nonlinear residuals reached their positive

248 extreme value and subsequently reached their negative extreme value before the water elevation

249 experienced its most substantial increase. The nonlinear residuals of P1, P2 and P3 reached their

250 positive extremes of 0.19 m, 0.14 m and 0.04 m, respectively. This resulted in the induction of

251 effects associated with the falling tide. The nonlinear residuals exhibited a decrease after Typhoon

252 Nida made landfall and reached their negative extremes near the time of the positive extremes in

253 storm surge elevation. Specifically, the negative extreme values of the nonlinear residuals at P1,

254 P2 and P3 were -0.43 m, -0.29 m and -0.11 m, respectively. The nonlinear effect within the PRE

255 exhibited a notable increase from the exterior towards the the interior. Additionally, the positive

256 extreme values of nonlinear residuals for P4 and P5 were 0.16 m and 0.14 m, respectively. While

257 the negative extreme values of nonlinear residuals for P4 and P5 were both -0.29 m each. These

258 findings indicate that the overall impact of Typhoon Nida was characterized by a greater decrease

259 in nonlinear residuals than any increase.

260 We are primarily concerned with the increase in water level that contributes the most

261 significant influence on the elevation of the storm tide. The contributions of the storm surge

262 elevation, the tide elevation, the practical storm surge elevation, and the nonlinear residual to the

263 storm tide elevation are calculated from five points in the PRE region, as shown in Table 2. It is

264 evident from our findings that both storm surge and the tide make positive contributions to the

265 elevation of storm tide. In contrast, the nonlinear residuals exert a negative influence on the storm

266 tide elevation. The analysis identified the contribution of practical storm surge to storm tide at P1

267 is identified as the most significant among the five points. Especially, the nonlinear effect at P2 is

268 the most pronounced when compared to other points.

删除[Linxu Huang]: are

删除[Linxu Huang]: residual levels

删除[Linxu Huang]: total

删除[Linxu Huang]: T+S

删除[Linxu Huang]: levels

删除[Linxu Huang]: significantly

删除[Linxu Huang]: d

删除[Linxu Huang]: parts

删除[Linxu Huang]: yang

删除[Linxu Huang]: the typhoon

删除[Linxu Huang]: residual levels

删除[Linxu Huang]: peaked

删除[Linxu Huang]: at

删除[Linxu Huang]: maximum

删除[Linxu Huang]: maximum

删除[Linxu Huang]: level

删除[Linxu Huang]: residual levels

删除[Linxu Huang]: maxima

删除[Linxu Huang]: ,

删除[Linxu Huang]: which

删除[Linxu Huang]: turn induced

删除[Linxu Huang]: residual levels

删除[Linxu Huang]: decreased

删除[Linxu Huang]: maxima

删除[Linxu Huang]: peak

删除[Linxu Huang]: level

删除[Linxu Huang]: residual levels

删除[Linxu Huang]: of

删除[Linxu Huang]: significant

删除[Linxu Huang]: its

删除[Linxu Huang]: maximum

删除[Linxu Huang]: level

删除[Linxu Huang]: ,

删除[Linxu Huang]: w

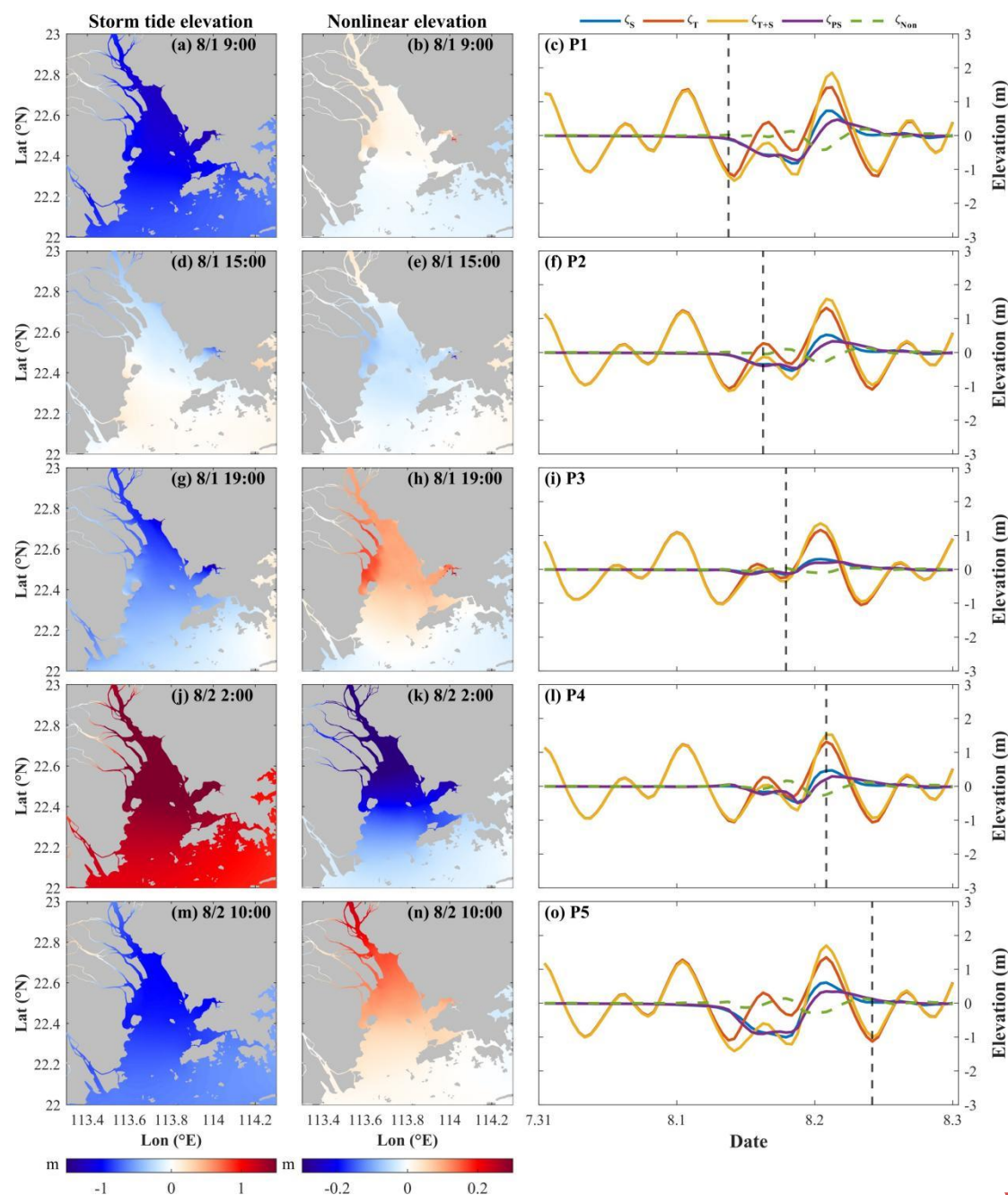
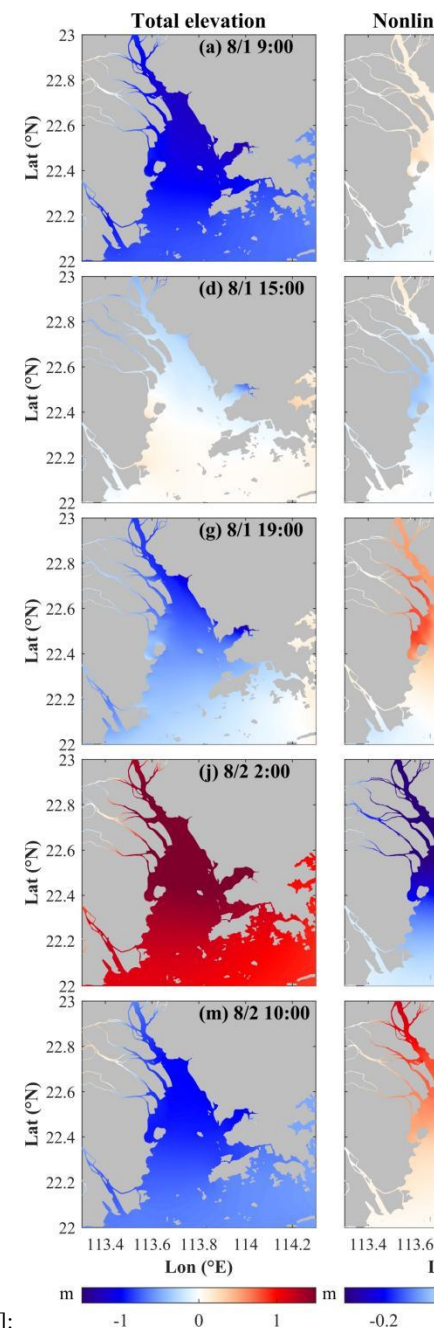


Figure 4. Storm tide elevation (left) and nonlinear elevation (middle) at different tidal phase; Time series of water elevation for P1, P2, P3, P4 and P5 locations (right); The dashed line indicates the time corresponding to the time on the left and middle graphs.

To emphasize the importance of the nonlinear effect, we have calculated the ratio of the nonlinear residuals to the storm surge and compared it with the ratio of the nonlinear residuals to the practical storm surge, as shown in Table 3. The ratio of the nonlinear residuals to the storm surge represents the extent to which the nonlinear effect amplifies or diminishes the direct impact of the storm surge. Meanwhile, the ratio of the nonlinear residuals to the practical storm surge provides insight into the extent to which the nonlinear effect contributes to the practical storm surge. It is observed that, among all five points, the influence of storm surges on water elevation is relatively minor at P3 due to nonlinear effects. However, the effects in question have an almost



删除[Linxu Huang]:

删除[Linxu Huang]: Total level

删除[Linxu Huang]: -

删除[Linxu Huang]: level

删除[Linxu Huang]: levels

删除[Linxu Huang]: pure

删除[Linxu Huang]: pure

删除[Linxu Huang]: represents how much

删除[Linxu Huang]: contribution

删除[Linxu Huang]: is made by the nonlinear effect

删除[Linxu Huang]: Among

删除[Linxu Huang]: it is observed that at P3, there is a

删除[Linxu Huang]: pure

删除[Linxu Huang]: there is

57% negative impact on practical storm surges. Notably, at P2, there is a significantly negative contribution from nonlinear effects amounting to nearly 98%. This suggests that, in comparison to other points, P2 is subject to a more pronounced influence from storm surges, which can be considered to be a form of practical storm surges.

Table 2. The contribution to the storm tide elevation at the maximum moment of storm tide,

Stations	<u>Storm surge</u> (%)	Tide (%)	Practical <u>storm</u> surge (%)	Nonlinear effect (%)
P1	39.17	76.87	23.13	-16.05
P2	33.05	83.35	16.65	-16.40
P3	22.36	85.80	14.20	-8.16
P4	30.79	80.82	19.18	-11.61
P5	35.72	79.61	20.39	-15.33

Table 3. The contribution of the nonlinear effect at the maximum moment of storm tide

Stations	$\zeta_{\text{Non}} / \zeta_{\text{S}}$ (%)	$\zeta_{\text{Non}} / \zeta_{\text{PS}}$ (%)
P1	-40.97	-69.38
P2	-49.61	-98.47
P3	-36.49	-57.46
P4	-37.71	-60.54
P5	-42.91	-75.17

3.3 The characteristics of storm surge by different typhoon landfall time

The primary factors contributing to tide-surge interactions are the alteration of tidal phase, caused by storm surge and the modulation of storm surges due to tides (Feng et al., 2019; Zheng et al., 2020). Accordingly, the typhoon landfall times were modified in order to examine the characteristics of storm surges occurring during different tidal phases. The nonlinear effects are subject to variation when typhoons make landfall at different tidal phases (Pandey and Rao, 2019). As shown in Fig 5, the practical storm surge at P1 shows minimal changes with different typhoon landfall times. When the positive increase in water elevation caused by storm surge coincides with the HHW tidal phase, the positive extreme values are smallest at each of the five points. The nonlinear residuals exhibited a decrease, in both positive and negative extreme values from the inner to the outer regions of Lingding Bay. However, when the positive increase in water elevation due to storm surge coincides with HLW tidal phase, which is equivalent to an advance in landfall time by 6 h, it results in a significantly greater positive extreme value of the practical surge elevation compared to others, as shown in Table 4. The influence of tides on storm tide elevation is more pronounced than that of storm surges, while the nonlinear effect exhibits a negative contribution (see Table 6). When a positive increase in water elevation resulting from a storm surge coincides with the LHW tidal phase, corresponding to an 11 h advance in landfall time, the positive extreme value of the practical storm surge shows minimal variation compared to when it coincides with the HHW tidal phase. Both storm surges and tides contribute positively to the storm tide elevation. However, the increase in water elevation due to the storm surge is greater than that due to the tide. Consequently, the nonlinear effect shows a negative contribution resulting in a reduction in water elevation (see Table 5). When the positive increase in water elevation from a storm surge coincides with LLW tidal phase, occurring at the landfall time of

Typhoon Nida advanced by 16 h, the contribution of practical storm surge to the storm tide elevation is negative. Meanwhile, the contributions from the nonlinear effect are positive (see Table 6).

删除[Linxu Huang]: total water level
 删除[Linxu Huang]: tide and the
 删除[Linxu Huang]: 4

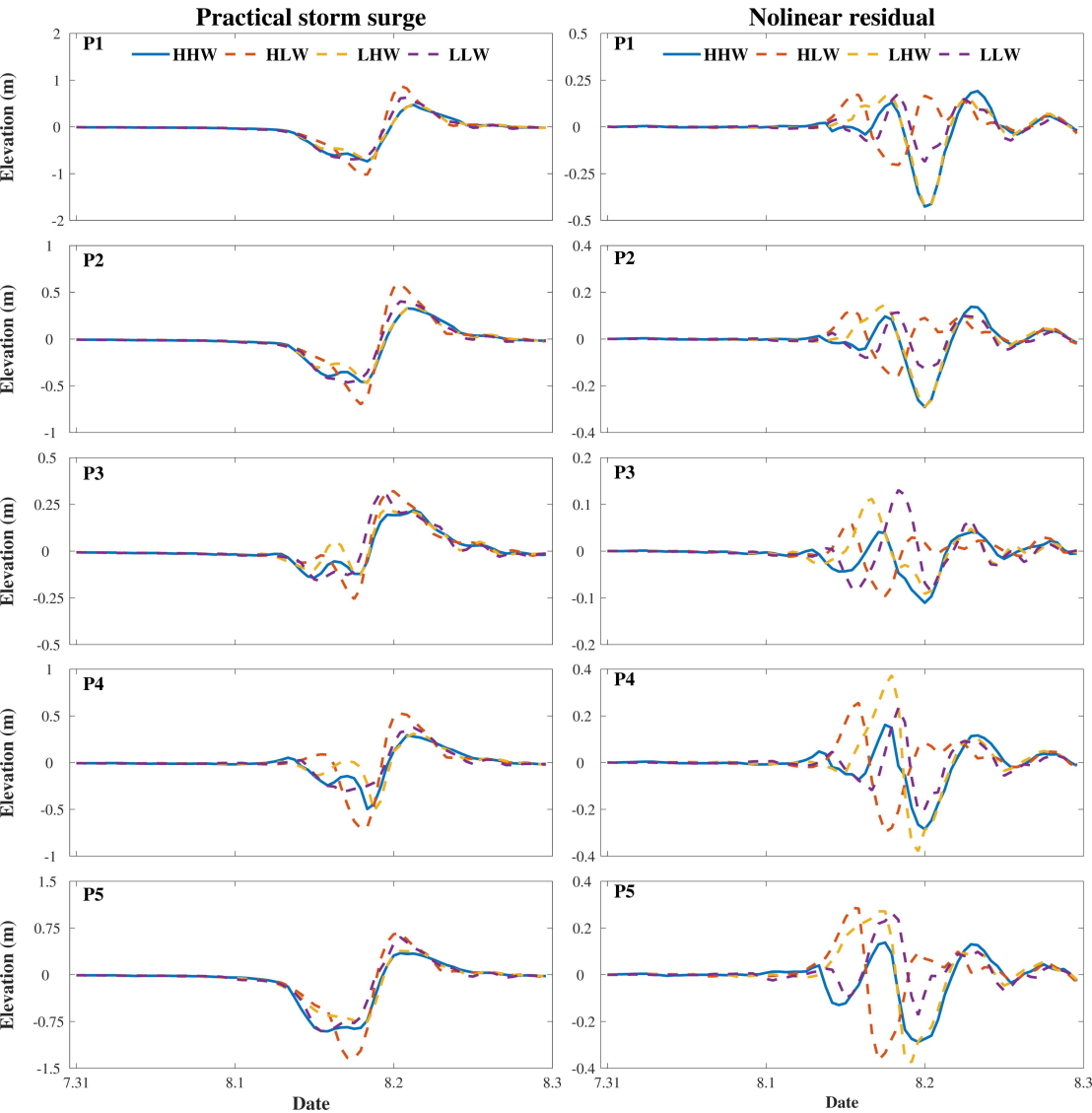


Figure 5. Time series of practical storm surge elevation (left) and nonlinear elevation (right) induced by different landfall time forcing at P1, P2, P3, P4 and P5

Table 4. Extreme value of practical storm surge elevation caused by different landfall time forcing at P1, P2, P3, P4 and P5

Stations	Negative extreme value of practical storm surge elevation (m)				Positive extreme value of practical storm surge elevation (m)			
	HHW	HLW	LHW	LLW	HHW	HLW	LHW	LLW
P1	-0.74	-1.02	-0.72	-0.63	0.47	0.88	0.49	0.63
P2	-0.46	-0.70	-0.47	-0.46	0.33	0.59	0.35	0.40
P3	-0.14	-0.26	-0.13	-0.16	0.22	0.32	0.23	0.31
P4	-0.50	-0.70	-0.52	-0.30	0.29	0.53	0.31	0.37
P5	-0.91	-1.34	-0.79	-0.90	0.35	0.67	0.38	0.60

Table 5. Extreme value of nonlinear elevation caused by different landfall time forcing at P1, P2, P3, P4 and P5

Stations	Negative extreme value of nonlinear elevation				Positive extreme value of nonlinear elevation			
	(m)				(m)			
	HHW	HLW	LHW	LLW	HHW	HLW	LHW	LLW
P1	-0.43	-0.20	-0.43	-0.19	0.19	0.17	0.17	0.18
P2	-0.29	-0.16	-0.29	-0.13	0.14	0.13	0.15	0.11
P3	-0.11	-0.10	-0.09	-0.09	0.04	0.06	0.11	0.13
P4	-0.29	-0.3	-0.38	-0.21	0.16	0.26	0.37	0.23
P5	-0.29	-0.36	-0.37	-0.17	0.14	0.29	0.27	0.26

Table 6. Contribution of the storm tide elevation when the maximum storm surge coincides with the different tidal phases at P1, P2, P3, P4 and P5

Stations	Practical surge (%)				Nonlinear effect (%)			
	HHW	HLW	LHW	LLW	HHW	HLW	LHW	LLW
P1	23.13	193.17	51.47	-174.92	-16.05	22.20	-36.87	27.84
P2	16.65	224.68	49.68	-68.08	-16.40	25.94	-50.12	20.09
P3	14.20	354.88	57.33	-36.91	-8.16	19.24	-24.73	10.67
P4	19.18	172.11	51.23	-67.90	-11.61	14.37	-35.65	25.29
P5	20.39	207.21	55.94	-133.17	-15.33	18.79	-32.97	1.06

Table 7. The contribution of the nonlinear effect when the maximum storm surge coincides with the different tidal phases at P1, P2, P3, P4 and P5

Stations	$\zeta_{\text{Non}} / \zeta_{\text{S}}$ (%)				$\zeta_{\text{Non}} / \zeta_{\text{PS}}$ (%)			
	HHW	HLW	LHW	LLW	HHW	HLW	LHW	LLW
P1	-40.96	12.98	-41.74	-13.73	-69.38	11.49	-71.63	-15.92
P2	-49.61	13.05	-50.22	-22.78	-98.47	11.55	-100.89	-29.51
P3	-36.49	5.73	-30.14	-22.43	-57.46	5.42	-43.14	-28.91
P4	-37.71	9.11	-41.03	-27.14	-60.54	8.35	-69.59	-37.25
P5	-42.91	9.97	-37.08	-0.79	-75.17	9.07	-58.94	-0.80

Above all, the practical storm surge elevation and the nonlinear elevation are significantly modulated by tidal forces, particularly in shallow water areas (Zhang et al., 2017; Zhang et al., 2019; Zhang et al, 2021). The practical storm surge exerts the greatest contribution to the storm tide elevation when the maximum of the storm surge coincides with the HLW tidal phase, as opposed to other phases. The nonlinear effect is negative during high tide (HHW and LHW) and positive during low tides (HLW and LLW) (Horsburgh and Wilson, 2007). The tidal contribution to the storm tide exceeds the that of the storm surge when the maximum of storm surges coincides with high tides. Conversely, the contribution of tides is less pronounced than that of the storm surge when the maximum of storm surges coincides with low tides. Notably, when the maximum of storm surges coincides with the LHW tidal phase, the contribution of the nonlinear effect is the greatest compared to other tidal phases (see Table 6). When the landfall time coincides with different tidal phases, the positive extreme value of nonlinear residuals changes little, whereas the

删除[Linxu Huang]: total

删除[Linxu Huang]: pure

删除[Linxu Huang]: caused by different landfall time forcing

删除[Linxu Huang]: importance

删除[Linxu Huang]: by different landfall time forcing

删除[Linxu Huang]: level

删除[Linxu Huang]: level

删除[Linxu Huang]: make

删除[Linxu Huang]: most

删除[Linxu Huang]: total

删除[Linxu Huang]: pure

删除[Linxu Huang]: than

删除[Linxu Huang]: contribution

删除[Linxu Huang]: pure

删除[Linxu Huang]: smaller

删除[Linxu Huang]: contribution

删除[Linxu Huang]: pure

删除[Linxu Huang]: pure

删除[Linxu Huang]: 4

删除[Linxu Huang]: positive

删除[Linxu Huang]: but

negative extreme value of nonlinear residuals changes significantly as shown in Table 5. As shown in Table 6, the practical storm surge makes the greatest contribution when the maximum of the storm surge coincides with the LHW tidal phase, compared to other tidal phases. The nonlinear effect has the greatest impact when the maximum of the storm surge coincides with the HLW tidal phase. A comparison of the ratios reveals that both the ratio of nonlinear residuals to the storm surge and the ratio of nonlinear residuals to the practical storm surge are positive when the maximum storm surge coincides with HLW tidal phase. Conversely, they are negative during other tidal phases (see Table 7). This indicates that an increase in water elevation due to nonlinear effects becomes significant only when the maximum of storm surge coincides with HLW tidal phase.

3.4 Dynamic mechanism of nonlinear residual levels caused by Typhoon Nida

To further analyze the source of the tide-surge interaction and its nonlinear effects, we utilized the formula proposed by (Yang et al., 2019) for calculating these nonlinear terms. As shown in Fig 2, five representative points were selected to illustrate the nonlinear effects of tide-surge interactions in the PRE.

$$\begin{aligned} \frac{\partial U_{NS}}{\partial t} + \psi_x(U_{NS}, V_{NS}) - fV_{NS} - \tau_x^S - \tau_x^B &= -g \frac{\partial \zeta_I}{\partial x} \\ \frac{\partial V_{NS}}{\partial t} + \psi_y(U_{NS}, V_{NS}) + fU_{NS} - \tau_y^S - \tau_y^B &= -g \frac{\partial \zeta_I}{\partial y} \end{aligned} \quad (10)$$

The calculated results of nonlinear dynamic terms, including the nonlinear local acceleration term $\frac{\partial U_{NS}}{\partial t}$ and $\frac{\partial V_{NS}}{\partial t}$, the nonlinear convection term ψ_x, ψ_y , the nonlinear Coriolis force term fU_{NS}, fV_{NS} , the nonlinear wind stress term τ_x^S, τ_y^S , and the nonlinear bottom friction term τ_x^B, τ_y^B at each points in x and y direction are shown in Fig 6:

In the eastward direction (x component) at P1, the nonlinear local acceleration term plays a dominant role, with some contribution from the nonlinear bottom friction term. It is important to note that this phenomenon occurs within Lingding Bay. It is concluded that the effects of nonlinear advection and Coriolis force are deemed negligible. As Typhoon Nida approached Lingding Bay after 18:00 on 1 August 2016, the local acceleration term exhibited an increase, reaching a positive extreme at 00:00 on 2 August 2016, which is similar to the Coriolis term. The advection term reached its positive extreme one hour later, occurring simultaneously with the negative extreme of the nonlinear residuals. Although the wind stress term is minimal, the bottom friction term reached its negative extreme at 2:00 on 2 August 2016, coinciding with the storm surge reaching its positive extreme. In the northward direction (y component), the amplitude of nonlinear local acceleration remains large; however, it is surpassed by the leading role played by the nonlinear advection term which reached its positive extreme at 2:00 on 2 August 2016.

In the eastward direction at P2, the values of the various nonlinear terms were relatively small, contributing little to the overall nonlinear effect. With the wind stress term playing a minor role among all nonlinear terms. However, in the northward direction, the local acceleration term is the dominant factor. The value reached its negative extreme at 22:00 on 1 August 2016, and reached its positive extreme at 6:00 on 2 August 2016.

In the eastward direction at P3, the nonlinear Coriolis term was the dominant factor, with

values reaching their positive extreme at 23:00 on 1 August 2016. Concurrently, both the nonlinear advection term and the local acceleration term reached their positive extremes, with each term making a significantly contribution. Among all the nonlinear terms, the wind stress plays a minor role.

删除[Linxu Huang]: reached
删除[Linxu Huang]: its
删除[Linxu Huang]: maximum
删除[Linxu Huang]: maximums

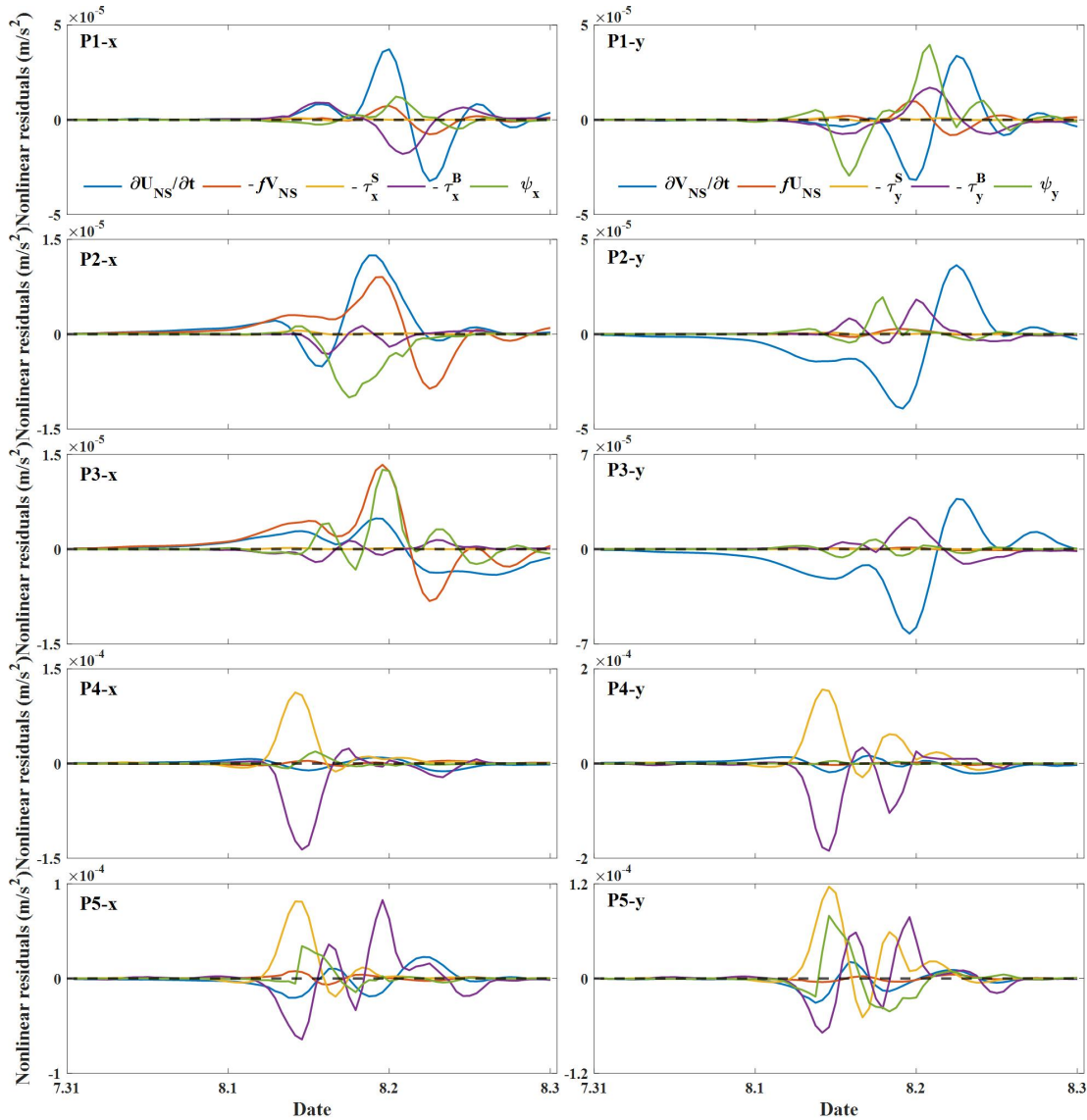


Figure 6. Time series of the nonlinear components of Typhoon Nida at P1, P2, P3, P4 and P5 in x direction (left) and y direction (right)

设置格式[Linxu Huang]: 字体: 倾斜
设置格式[Linxu Huang]: 字体: 倾斜
删除[Linxu Huang]: located
删除[Linxu Huang]: is located
删除[Linxu Huang]: strong
删除[Linxu Huang]: tide-surge
删除[Linxu Huang]: maximum
删除[Linxu Huang]: The
删除[Linxu Huang]: more important

Given that P4 is situated in the northern part of Qi'ao Island and P5 in Shenzhen Bay, these two points present areas of significant nonlinear effect of tide-surge interaction within the PRE region. As shown in Fig 7, in the eastward direction at P4, the nonlinear wind stress term plays a leading role and reached its positive extreme at 14:00 on 2 August 2016. It is also notable that the nonlinear bottom friction term is also significant. In the northward direction at P4, both the nonlinear wind stress and bottom friction terms contribute to the nonlinear effect. In the eastward direction at P5, the wind stress and bottom friction terms are of greater significance than the other terms.

401 About all points, the results indicate that the gradient of the nonlinear residuals was stronger
 402 in the northerly direction than in the easterly direction (Hu et al., 2023), with the exception of the
 403 nonlinear Coriolis term. This study focuses on analyzing storm surges induced by Typhoon Nida
 404 using a two-dimensional (2D) model with high regulation unstructured grid, which enhances both
 405 accuracy and robustness of our conclusions. The establishment of direct mathematical
 406 relationships between nonlinear residuals and dynamic terms through theoretical derivation
 407 provides valuable insights. It was found that the nonlinear acceleration term mainly contributes to
 408 the top of the bay, indicating a strong interaction between tidal current and storm-induced current
 409 (Song et al., 2020). Additionally, wind stress also affected the tide-surge interaction since the H
 410 was in the denominator of wind stress term, especially in shallow water area, such as the northern
 411 part of Qi'ao Island and Shenzhen Bay. Furthermore, it is noted that shallow water effects are
 412 more significant in Shenzhen Bay due to the restricted water depth over tidal flats (Zheng et al.,
 413 2020).
 414
 415 **3.4 Dynamic mechanism of the nonlinear residual levels influenced by different**
 416 **typhoon landfall time**
 417 To investigate the nonlinear momentum characteristics resulting from different tidal forcing,
 418 the nonlinear momentum terms were calculated. When the maximum increase in water elevation
 419 caused by storm surge coincides with the HLW tidal phase, the temporal changes of the nonlinear
 420 residuals are shown in Fig 7. In the eastward direction at P1, the dominant factor is the nonlinear
 421 local acceleration term, with some contribution from the nonlinear bottom friction term.
 422 Furthermore, the effects of nonlinear advection and Coriolis force also make significant
 423 contributions. In the northward direction, while the amplitude of the nonlinear local acceleration
 424 term remains considerable, it is surpassed by the influence of the nonlinear advection term. Both
 425 in x component and y component, the wind stress terms exhibit weak impact and can be neglected.
 426 In the eastward direction at P2, the values of various nonlinear terms were relatively small,
 427 contributing little to the nonlinear effect. Furthermore, the wind stress plays a minor role among
 428 all nonlinear terms. The nonlinear Coriolis term contributes to positive nonlinear residuals,
 429 whereas the advection term and the bottom friction term contribute negatively to nonlinear
 430 residuals. However, in the northward direction, the local acceleration term plays a leading role and
 431 reaches its negative extreme in nonlinear residuals at 16:00 on 1 August 2016. In the eastward
 432 direction at P3, the nonlinear Coriolis and nonlinear advection terms make some contributions.
 433 However, in the northward direction at P3, the dominant term is the nonlinear local acceleration
 434 term, with additional contributions from the bottom friction and nonlinear advection terms. The
 435 wind stress plays a minor role among all nonlinear terms. In the eastward direction at P4, the
 436 nonlinear bottom friction term plays a dominant role, reaching its negative extreme at 18:00 on 1
 437 August 2016. Following closely behind is the nonlinear wind stress term, which reached its
 438 positive extreme at 17:00 on 1 August 2016. In the northward direction at P4, both the nonlinear
 439 wind stress and bottom friction terms contribute to the nonlinear effect. Specifically, while the
 440 bottom friction term make a negative contribution to the nonlinear residuals, the wind stress
 441 contributes positively. The wind stress term reached its positive extreme at 17:00 on 1 August
 442 2016, and the bottom friction term reached its negative extreme at the same time. In the eastward
 443 direction at P5, the wind stress and bottom friction terms are of greater significance than the other
 444 terms. In the northward direction at P5, the wind stress term and bottom friction term also exerted

删除[Linxu Huang]: level

删除[Linxu Huang]: levels

删除[Linxu Huang]: the

删除[Linxu Huang]: because of limited

删除[Linxu Huang]:

删除[Linxu Huang]: we calculated

删除[Linxu Huang]: level

删除[Linxu Huang]: pure

删除[Linxu Huang]: The

删除[Linxu Huang]: although

删除[Linxu Huang]: large

设置格式[Linxu Huang]: 字体: 倾斜

删除[Linxu Huang]: -

设置格式[Linxu Huang]: 字体: 倾斜

删除[Linxu Huang]: -

删除[Linxu Huang]: directions

删除[Linxu Huang]: ,

删除[Linxu Huang]: and

删除[Linxu Huang]: while

删除[Linxu Huang]: maximum

删除[Linxu Huang]: leading

删除[Linxu Huang]: and reached

删除[Linxu Huang]: maximum

删除[Linxu Huang]: nolinear

删除[Linxu Huang]: maximum

删除[Linxu Huang]: maximum

删除[Linxu Huang]: maximum

删除[Linxu Huang]: more important

删除[Linxu Huang]: dominated

a dominant influence on the nonlinear residuals. Moreover, the absolute value of the positive extreme of the wind stress term is greater than that of the negative extreme. The advection term was so insignificant that it was recorded as negligible, resulting in a discontinuous time series.

删除[Linxu Huang]: wind stress term's
删除[Linxu Huang]: maximum
删除[Linxu Huang]: absolute value of bottom friction term's
删除[Linxu Huang]: maximum
删除[Linxu Huang]: small

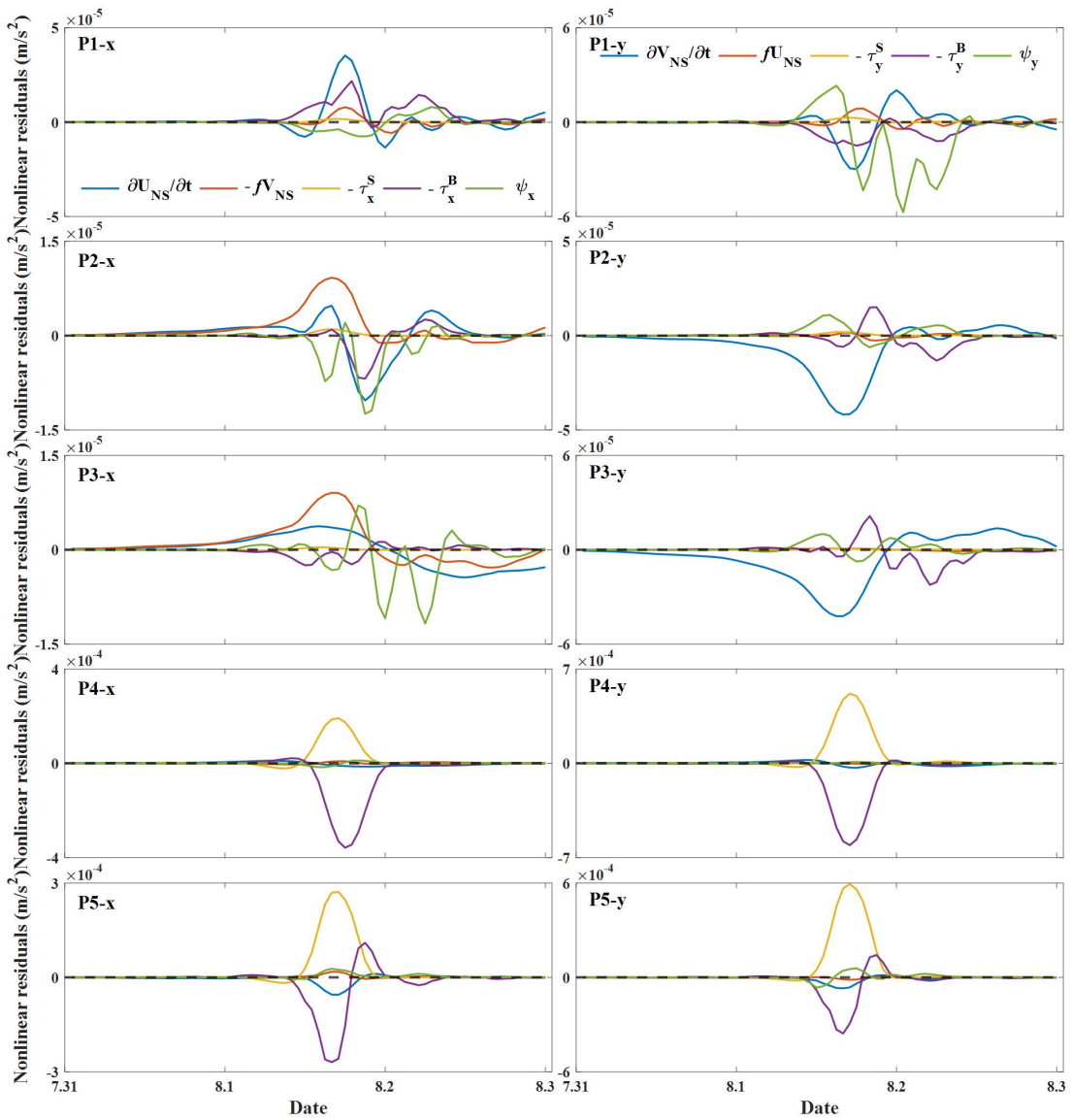


Figure 7. Time series of the nonlinear components at P1, P2, P3, P4 and P5 in x direction (left) and y direction (right) when the maximum storm surge coincides with the HLW tidal phase

设置格式[Linxu Huang]: 字体: 倾斜
设置格式[Linxu Huang]: 字体: 倾斜

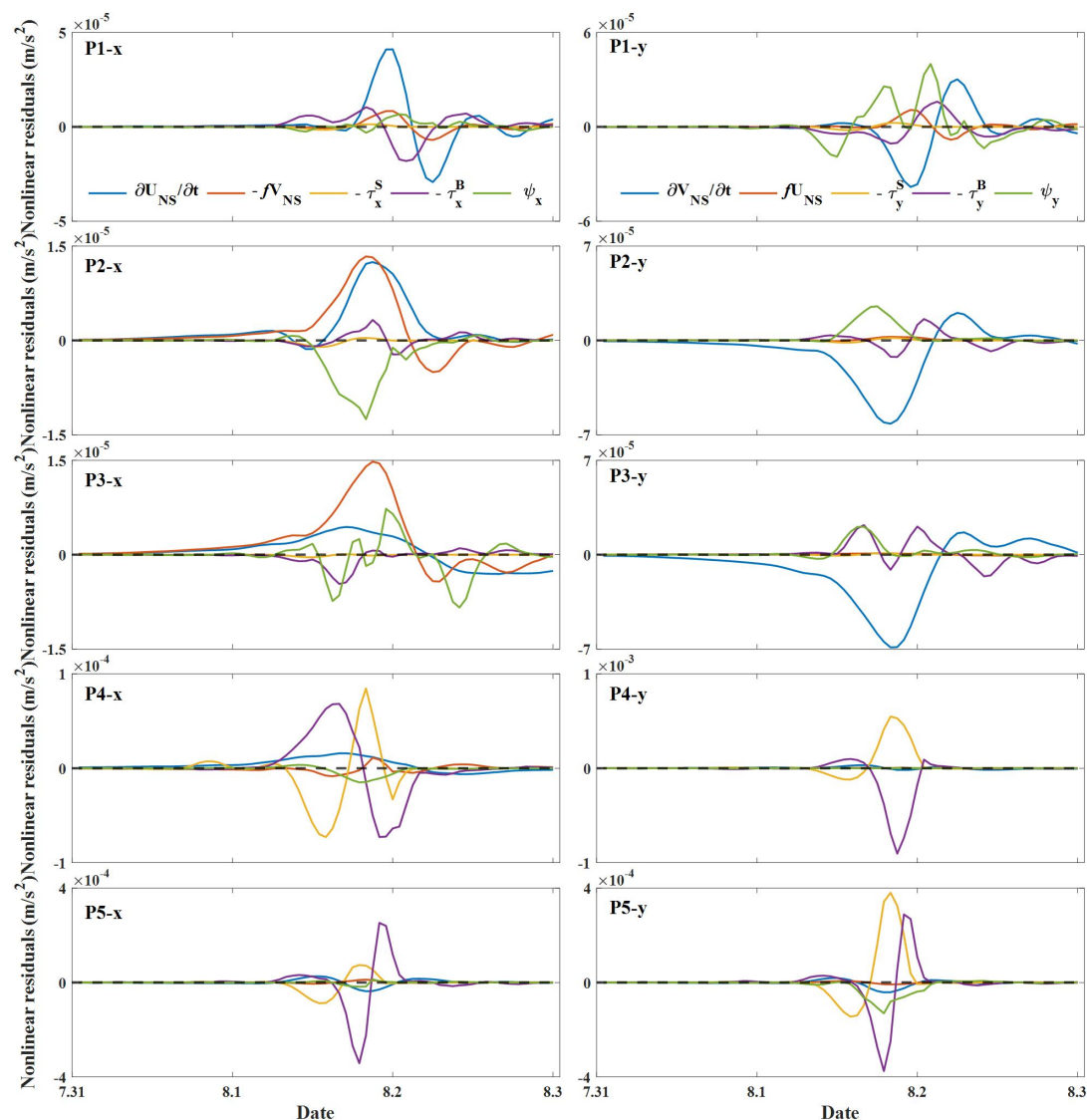


Figure 8. Time series of the nonlinear components at P1, P2, P3, P4 and P5 in x direction (left) and y direction (right) when the maximum storm surge coincides with the LHW tidal phase

When the maximum increase in water elevation caused by storm surge coincides with the LHW tidal phase, Fig. 8 illustrates the time series changes of the nonlinear residuals. In the eastward direction at P1, the nonlinear local acceleration term is also the most significant contributor, followed by the nonlinear bottom friction term, which represents the second-largest contribution. Nonlinear advection and Coriolis force exert a considerable influence on the nonlinear residuals. In the northward direction, the nonlinear local acceleration term and the nonlinear advection term exert a major contributions. Both in the x component and y component, the wind stress term is weak and can be considered negligible. In the eastward direction at P2, both the bottom friction term and the wind stress term are significantly smaller compared to other terms. The positive nonlinear residuals are contributed by nonlinear local acceleration term while the negative ones are result of contributions from the nonlinear advection term and bottom friction term. However, in the northward direction at P2, it is observed that the nonlinear local acceleration term plays a leading role and reached its negative extreme value at 20:00 on 1 August 2016. In the eastward direction at P3, the nonlinear Coriolis term dominates the nonlinear residuals, while the

设置格式[Linxu Huang]: 字体: 倾斜

设置格式[Linxu Huang]: 字体: 倾斜

删除[Linxu Huang]: pure

删除[Linxu Huang]: level

删除[Linxu Huang]: pure

删除[Linxu Huang]: ure

删除[Linxu Huang]: plays a leading role

删除[Linxu Huang]: as

删除[Linxu Huang]: The effects of nonlinear

删除[Linxu Huang]: also make significant contributions

删除[Linxu Huang]: make

设置格式[Linxu Huang]: 字体: 倾斜

删除[Linxu Huang]: -

设置格式[Linxu Huang]: 字体: 倾斜

删除[Linxu Huang]: -

删除[Linxu Huang]: are

删除[Linxu Huang]: exhibit

删除[Linxu Huang]: peak

nonlinear local acceleration term and the nonlinear advection term also make some contributions. However, in the northward direction at P3, the nonlinear local acceleration term is predominant, with the bottom friction term and the nonlinear advection term exerting influence. The wind stress and Coriolis effects are both minimal. In the eastward direction at P4, the nonlinear bottom friction term and the nonlinear wind stress term exert a greater impact than other terms. In the northward direction at P4, the nonlinear wind stress term and the bottom friction term significantly contribute to the nonlinear residuals. Notably, the absolute value of the extreme of the bottom friction term is greater than that of the wind stress term. The wind stress term reached its positive extreme at 20:00 on 1 August 2016, while the bottom friction term reached its negative extreme 1 h later. In the eastward direction at P5, the bottom friction term is the primary contributor, with the wind stress term providing a secondary contribution. In the northward direction at P5, the wind stress term and the bottom friction term exert a dominant influence on the nonlinear residuals, with the other terms having a negligible effect.

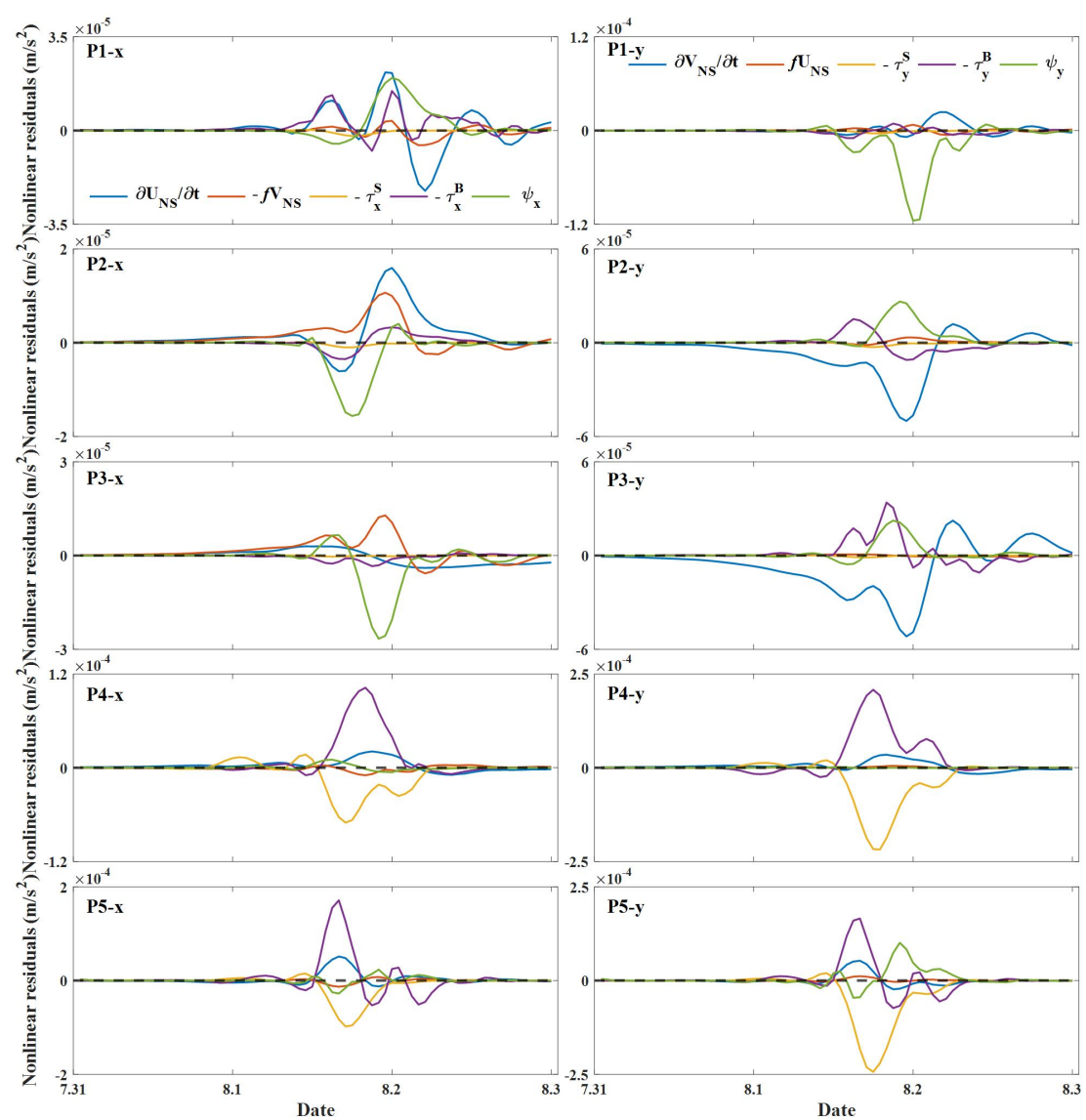


Figure 9. Time series of the nonlinear components at P1, P2, P3, P4 and P5 in x direction (left) and y direction (right) when the maximum storm surge coincides with the LLW tidal phase.

488 When the maximum increase in water elevation caused by the storm surge coincides with the
 489 LLW tidal phase, the time series changes of nonlinear residuals are shown in Fig 9. In the
 490 eastward direction at P1, the nonlinear local acceleration term, the advection term and the bottom
 491 friction term make major contributions. In the northward direction, the nonlinear advection term is
 492 the most significant contributor. Both in x component and y component, the wind stress term is
 493 relatively weak and can be considered negligible. In the eastward direction at P2, major
 494 contributions are made by the nonlinear local acceleration term, the Coriolis term, and the
 495 nonlinear advection term. However, in the northerly direction at P2, it is primarily influenced by
 496 the local acceleration term which reaches its negative extreme in nonlinear residuals at 23:00 on 1
 497 August 2016. Meanwhile, the advection term makes positive contrition to the nonlinear residuals,
 498 reaching its positive extreme at 22:00 on 1 August 2016. In the eastward direction at P3, the
 499 nonlinear advection term exerts the dominant influence, with the nonlinear Coriolis term also
 500 making some contributions. However, in the northward direction at P3, the nonlinear local
 501 acceleration term is predominant, with the bottom friction and the nonlinear advection term also
 502 contributing. The wind stress term and the Coriolis term are negligible in comparison. In the
 503 eastward direction at P4, the nonlinear bottom friction term and the nonlinear wind stress term
 504 make greater contributions than the other terms, with the nonlinear bottom friction term playing a
 505 leading role and providing a positive contribution to the nonlinear residuals. In the northward
 506 direction at P4, the nonlinear wind stress term and the bottom friction term make significant
 507 contribution to the nonlinear effect. The positive contribution of the bottom friction nearly
 508 balances the negative contribution of the wind stress. The wind stress reached its negative extreme
 509 at 19:00 on 1 August 2016, while the bottom friction term reached its positive extreme 1 h earlier.
 510 In the eastward direction at P5, the bottom friction term is the primary contributor, with the wind
 511 stress term making the second-largest contribution. In the northward direction at P5, the wind
 512 stress term is the most significant contributor, with the other terms making comparatively less
 513 impact.
 514 The occurrence of storm surges in the estuary area is subject to influence of both typhoons
 515 and tides. The interaction between these two forces on water elevation has been demonstrated in
 516 numerous studies. The elevation of storm surges in the PRE varies significantly depending on the
 517 tidal phase during which they occur. A compariosn of the nonlinear factors at those representative
 518 points across different tidal phases can make a better understanding of the mechanism underlying
 519 the tide-surge interaction. The analysis of the nonlinear terms in the nonlinear residuals revealed
 520 that when storm surges coincide with high tides (HHW and LHW), the nonlinear acceleration term
 521 predominantly affects the y component at P1. Conversely, when storm surges coincide with low
 522 tides (HLW and LLW) at P1, the nonlinear advection term is the dominant factor. In the eastward
 523 direction, the nonlinear acceleration term consistently plays a dominant role at P1. In the
 524 northward direction, both P2 and P3 are characterized by a predominant influence of the nonlinear
 525 acceleration term. In instances where storm surges occur concurrently with different tidal phases,
 526 the proportionate contribution of each nonlinear term remains almost unchanged, but their
 527 magnitudes vary. The results illustrate that the primary source of the tide-surge interaction
 528 nonlinear effects within the PRE is the effect of the tide's velocity. While in shallow water area,
 529 such as the northern part of Qi'ao Island and Shenzhen Bay, the tide-surge interaction nonlinear
 530 effects are predominantly influenced by a combination of wind and bottom friction.
 531

- 删除[Linxu Huang]: level
- 删除[Linxu Huang]: pure
- 删除[Linxu Huang]: plays a leading role
- 设置格式[Linxu Huang]: 字体: 倾斜
- 删除[Linxu Huang]: -
- 设置格式[Linxu Huang]: 字体: 倾斜
- 删除[Linxu Huang]: peak
- 删除[Linxu Huang]: and reaches
- 删除[Linxu Huang]: maximum
- 删除[Linxu Huang]: dominates
- 删除[Linxu Huang]: and
- 删除[Linxu Huang]: makes
- 删除[Linxu Huang]:
- 删除[Linxu Huang]: ly
- 删除[Linxu Huang]: contribute
- 删除[Linxu Huang]: ,
- 删除[Linxu Huang]: with the
- 删除[Linxu Huang]: balancing
- 删除[Linxu Huang]: maximum
- 删除[Linxu Huang]: maximum
- 删除[Linxu Huang]: plays a leading role
- 删除[Linxu Huang]: makes a more significant contributio ...
- 删除[Linxu Huang]: Storm
- 删除[Linxu Huang]: are
- 删除[Linxu Huang]: influenced
- 删除[Linxu Huang]: by
- 删除[Linxu Huang]: levels
- 删除[Linxu Huang]: many
- 删除[Linxu Huang]: Comparing
- 删除[Linxu Huang]: mechanism
- 删除[Linxu Huang]: Analysis
- 设置格式[Linxu Huang]: 字体: 倾斜
- 删除[Linxu Huang]: -
- 删除[Linxu Huang]: plays a leading role

532 **4. Conclusions**

533 An ADCIRC model has been utilized to simulate the storm surges in the PRE induced by
534 Typhoon Nida. Results from several numerical experiments investigating the interaction between
535 tides and storm surges indicate that when the tidal effect is incorporated, the simulations agree
536 well with observational data.

537 To study the characteristics of tide-surge interaction in the PRE, three types of model runs
538 were conducted, from which the ~~storm tide~~, the ~~astronomical tide~~, the ~~storm surge~~, the practical
539 storm surge and the ~~nonlinear~~ residual due to the tide-surge interaction were obtained. The results
540 show that, the storm surge is significantly modulated by the tide due to the tide-surge interaction.
541 A direct mathematical relationship between nonlinear ~~residuals~~ and dynamic influencing factors
542 has been established. This derivation includes the local acceleration term, the Coriolis force term,
543 the wind stress term, the bottom friction term and the nonlinear advection term. The nonlinear
544 momentum term can reflect the momentum response of different areas ~~within~~ the estuary to
545 nonlinear effect. The momentum equation facilitates the establishment of a relationship between
546 the nonlinear factors of tide-surge interactions and the underlying physical processes. ~~A~~
547 ~~comparison of~~ nonlinear factors at representative points from the inner to the outer bay, has
548 ~~demonstrated~~ that the local acceleration term and the nonlinear advection term ~~exert a~~
549 ~~predominant~~ influence ~~on~~ the nonlinear dynamics. However, in ~~the case of~~ Shenzhen Bay and the
550 northern part of Qi'ao Island, ~~it is~~ the wind stress term and the bottom friction term ~~that~~ emerge as
551 the dominant nonlinear factors.

552 To further investigate the relationship between ~~tidal~~ phases and storm surges, we adjusted the
553 landfall time of Typhoon Nida in our model simulations. The results shows that both the practical
554 storm surge and the nonlinear ~~residuals~~ are significantly modulated by tidal forces, especially in
555 shallow water areas. ~~In instances where the maximum of~~ storm surge coincides with high tides,
556 ~~the contribution of the tide to the storm tide is greater than that of the storm surge~~. Conversely, the
557 contribution of tides to the ~~storm tide~~ is less than ~~that of~~ the storm surge when the maximum of ~~the~~
558 ~~storm surge~~ coincides with low tides. The analysis revealed that the nonlinear effect of tide-surge
559 interaction is positive when the ~~maximum~~ of storm surge coincides with low tidal phase (LLW and
560 HLW). On the contrary, this nonlinear effect becomes negative when the ~~maximum of the~~ storm
561 surge coincides with high tidal phase (HHW and LHW). Notably, when the maximum of ~~storm~~
562 surges coincides with the LHW tidal phase, the contribution of the nonlinear effect is the greatest
563 ~~in comparison~~ to other tidal phases. The ratio of nonlinear residuals to the ~~storm surge~~ and the
564 ratio of the nonlinear residuals to the practical storm surge are both positive when the maximum of
565 the ~~storm surge~~ coincides with the HLW tidal phase, while the ratios during other tidal phases are
566 negative.

567 Although similar results were also presented in other studies (Song et al., 2020; Hu et al.,
568 2023), the discussions of nonlinear momentum for different tidal phases are still lacking. We
569 calculated the nonlinear terms to discuss the characteristics and mechanisms of tide-surge
570 interaction. When storm surges coincide with different tidal phases, the contribution ratio of each
571 nonlinear term remains almost unchanged, but their magnitudes ~~exhibit notable variation~~. The
572 results illustrate that the primary source of the tide-surge interaction nonlinear effects within the
573 PRE is the effect of the tide's velocity. ~~In areas of~~ shallow water, such as the northern part of Qi'ao
574 Island and Shenzhen Bay, the tide-surge interaction nonlinear effects are predominantly influenced

- 删除[Linxu Huang]: total water level
- 删除[Linxu Huang]: pure
- 删除[Linxu Huang]: level
- 删除[Linxu Huang]: pure
- 删除[Linxu Huang]: elevation
- 删除[Linxu Huang]: level
- 删除[Linxu Huang]: levels
- 删除[Linxu Huang]: in
- 删除[Linxu Huang]: By
- 删除[Linxu Huang]: comparing
- 删除[Linxu Huang]: , it
- 删除[Linxu Huang]: been shown
- 删除[Linxu Huang]: predominantly
- 删除[Linxu Huang]: tide
- 删除[Linxu Huang]: level
- 删除[Linxu Huang]: level
- 删除[Linxu Huang]: The tidal contribution to the total wa ...
- 删除[Linxu Huang]: pure
- 删除[Linxu Huang]: extreme total water level
- 删除[Linxu Huang]: contribution
- 删除[Linxu Huang]: pure
- 删除[Linxu Huang]: peak
- 删除[Linxu Huang]: pure
- 删除[Linxu Huang]: pure
- 删除[Linxu Huang]: peak
- 删除[Linxu Huang]: pure
- 删除[Linxu Huang]: compared
- 删除[Linxu Huang]: pure
- 删除[Linxu Huang]: pure
- 删除[Linxu Huang]: are different
- 删除[Linxu Huang]: While in
- 删除[Linxu Huang]: area

by a combination of wind and bottom friction.

Taking Typhoon Nida as a case study, the present research reveals the detailed characteristics of tide-surge interaction in the PRE. The present results of this study can provide valuable information for understanding the tide-surge interaction mechanism and improving storm surges prediction within the PRE. However, further studies on additional typhoon events may be needed, along with a comprehensive consideration of meteorological processes and the mechanisms of tidal-wave propagation within and outside the estuary, and the model system could still be improved in the future.

删除[Linxu Huang]: need

Data availability. The typhoon best track datasets used in this study is available from the CMA repository (<http://tcdata.typhoon.org.cn>). The tide gauge datasets used in this study are available from the authors on request.

Author contributions. LH, TZ, and SZ designed the study. LH conducted and made the analysis. All authors contributed to the discussion of the analysis and the final manuscript.

Competing interests. The contact author has declared that none of the authors has any competing interests.

Acknowledgements. We thank Hui Wang for him helpful discussions.

Financial support. This research was jointly funded by Independent research project of Southern Marine and Engineering Guangdong Laboratory (Zhuhai) (Grant No. SML2022SP301 and No. SML2022SP504); the National Natural Science Foundation of China (Grant No. 41976200, and 42206029); the Innovative Team Plan for Department of Education of Guangdong Province (No. 2023KCXTD015); the Guangdong Science and Technology Plan Project (Observation of Tropical marine environment in Yuexi), Guangdong Ocean University Scientific Research Program (Grant No. 060302032106).

Reference

- Bernier, N., and Thompson, K.: Tide-surge interaction off the east coast of Canada and northeastern United States, *J. Geophys. Res.-Oceans*, 112, <https://doi.org/10.1029/2006JC003793>, 2007.
- Egbert, G. D., and Erofeeva, S. Y.: Efficient inverse modeling of barotropic ocean tides. *J. Atmos. Ocean. Technol.*, 19, 183-204, [https://doi.org/10.1175/1520-0426\(2002\)019<0183:EIMOBO>2.0.CO;2](https://doi.org/10.1175/1520-0426(2002)019<0183:EIMOBO>2.0.CO;2), 2002.
- Feng, J., Jiang, W., Li, D., Liu, Q., Wang, H., and Liu, K.: Characteristics of tide–surge interaction and its roles in the distribution of surge residuals along the coast of China, *J. oceanogr.*, 75, 225-234, <https://doi.org/10.1007/s10872-018-0495-8>, 2019.
- Feng, X., Olabarrieta, M., and Valle-Levinson, A.: Storm-induced semidiurnal perturbations to surges on the US Eastern Seaboard, *Cont. Shelf. Res.*, 114, 54-71. <https://doi.org/10.1016/j.csr.2015.12.006>, 2016.
- Flather, R.: Storm surge Prediction Model for the Northern Bay of Bengal with Application to Cyclone Disaster in April 1991, *J. Phys. Oceanogr.*,

[https://doi.org/10.1175/1520-0485\(1994\)024<0172:ASSPMF>2.0.CO;2](https://doi.org/10.1175/1520-0485(1994)024<0172:ASSPMF>2.0.CO;2), 1994.
 Garratt, J.: Review of drag coefficients over oceans and continents, *Mon. Wea. Rev.*, 105, 915-929.
[https://doi.org/10.1175/1520-0493\(1977\)105<0915:RODCOO>2.0.CO;2](https://doi.org/10.1175/1520-0493(1977)105<0915:RODCOO>2.0.CO;2), 1977.
 Heaps, N.: Storm surges, 1967–1982, *Geophys. J. Int.*, 74, 331-376,
<https://doi.org/10.1111/j.1365-246X.1983.tb01883.x>, 1983.
 Holland, G. J.: An Analytic Model of the Wind and Pressure Profiles in Hurricanes. *Mon. Wea. Rev.*,
 108, 1212-1218. [https://doi.org/10.1175/1520-0493\(1980\)108<1212:AAMOTW>2.0.CO;2](https://doi.org/10.1175/1520-0493(1980)108<1212:AAMOTW>2.0.CO;2),
 1980.
 Horsburgh, K., and Wilson, C.: Tide-surge interaction and its role in the distribution of surge residuals
 in the North Sea, *J. Geophys. Res.-Oceans*, 112, <https://doi.org/10.1029/2006JC004033>, 2007.
 Hu, S., Liu, B., Hu, M., Yu, X., Deng, Z., Zeng, H., and Li, D.: Quantification of the nonlinear
 interaction among the tide, surge and river in Pearl River Estuary, *Estuar. Coast Shelf S.*, 290,
 108415, <https://doi.org/10.1016/j.ecss.2023.108415>, 2023.
 Idier, D., Dumas, F., and Muller, H.: Tide-surge interaction in the English Channel, *Nat. Hazards Earth*
Syst. Sci., 12, 3709-3718, <https://doi.org/10.5194/nhess-12-3709-2012>, 2012.
 Johns, B., Rao, A., Dubinsky, Z., and Sinha, P.: Numerical modelling of tide-surge interaction in the
 Bay of Bengal, *Philosophical Transactions of the Royal Society of London. Series A,*
Mathematical Physical Sciences, 313, 507-535. <https://doi.org/10.1098/rsta.1985.0002>, 1985.
 Lu, X., Yu, H., Ying, M., Zhao, B., and Wan, R.: Western North Pacific Tropical Cyclone Database
 Created by the China Meteorological Administration, *Adv. Atmos. Sci.*, 38, 690-699,
<https://doi.org/10.1007/s00376-020-0211-7>, 2021.
 Luettich, R. A., Westerink, J. J., and Scheffner, N. W.: ADCIRC: an advanced three-dimensional
 circulation model for shelves, coasts, and estuaries. Report 1, Theory and methodology of
 ADCIRC-2DDI and ADCIRC-3DL, 1992.
 Olbert, A. I., Nash, S., Cunnane, C., and Hartnett, M. (2013). Tide–surge interactions and their effects
 on total sea levels in Irish coastal waters, *Ocean Dynam.*, 63, 599-614,
<https://doi.org/10.1007/s10236-013-0618-0>, 2013.
 Pandey, S., and Rao, A.: Impact of approach angle of an impinging cyclone on generation of storm
 surges and its interaction with tides and wind waves, *J. Geophys. Res.-Oceans*, 124,
 7643-7660, <https://doi.org/10.1029/2019JC015433>, 2019.
 Quinn, N., Atkinson, P. M., and Wells, N. C.: Modelling of tide and surge elevations in the Solent and
 surrounding waters: The importance of tide–surge interactions, *Estuar. Coast Shelf S.*, 112,
 162-172, <https://doi.org/10.1016/j.ecss.2012.07.011>, 2012.
 Rego, J. L., and Li, C.: Nonlinear terms in storm surge predictions: Effect of tide and shelf geometry
 with case study from Hurricane Rita, *J. Geophys. Res.-Oceans*, 115,
<https://doi.org/10.1029/2009JC005285>, 2010.
 Rossiter, J. R.: Interaction between tide and surge in the Thames, *Geophys. J. Int.*, 6, 29-53.
<https://doi.org/10.1111/j.1365-246x.1961.tb02960.x>, 1961.
 Song, H., Kuang, C., Gu, J., Zou, Q., Liang, H., Sun, X., and Ma, Z.: Nonlinear tide-surge-wave
 interaction at a shallow coast with large scale sequential harbor constructions, *Estuar. Coast*
Shelf S., 233, 106543, <https://doi.org/10.1016/j.ecss.2019.106543>, 2020.
 Valle-Levinson, A., Olabarrieta, M., and Valle, A.: Semidiurnal perturbations to the surge of Hurricane
 Sandy, *Geophys. Res. Lett.*, 40, 2211-2217, <https://doi.org/10.1002/grl.50461>, 2013.
 Westerink, J. J., Blain, C. A., Luettich, R. A., and Scheffner, N. W.: ADCIRC: An Advanced

662 Three-dimensional Circulation Model for Shelves, Coasts and Estuaries, Report 2-User's
 663 Manual for ADCIRC-2DDI: US Army Corps of Engineers Washington, DC, 1992
 664 Wolf, J.: Interaction of tide and surge in a semi-infinite uniform channel, with application to surge
 665 propagation down the east coast of Britain, *Applied Mathematical Modelling*, 2, 245-253,
 666 [https://doi.org/10.1016/0307-904X\(78\)90017-3](https://doi.org/10.1016/0307-904X(78)90017-3), 1978.
 667 Xu, J., Zhang, Y., Cao, A., Liu, Q., and Lv, X.: Effects of tide-surge interactions on storm surges along
 668 the coast of the Bohai Sea, Yellow Sea, and East China Sea, *Sci. China Earth Sci.*, 59,
 669 1308-1316, <https://doi.org/10.1007/s11430-015-5251-y>, 2016.
 670 Yang, W., Yin, B., Feng, X., Yang, D., Gao, G., and Chen, H.: The effect of nonlinear factors on
 671 tide-surge interaction: A case study of Typhoon Rammasun in Tieshan Bay, China. *Estuar.*
 672 *Coast Shelf S*, 219, 420-428, <https://doi.org/10.1016/j.ecss.2019.01.024>, 2019.
 673 Zhang, H., Cheng, W., Qiu, X., Feng, X., and Gong, W.: Tide-surge interaction along the east coast of
 674 the Leizhou Peninsula, South China Sea, *Cont. Shelf. Res.*, 142, 32-49.
 675 <https://doi.org/10.1016/j.csr.2017.05.015>, 2017.
 676 Zhang, W., Teng, L., Zhang, J., Xiong, M., and Yin, C.: Numerical study on effect of tidal phase on
 677 storm surge in the South Yellow Sea, *J. Ocean. Limnol.*, 37, 2037-2055,
 678 <https://doi.org/10.1007/s00343-019-8277-8>, 2019.
 679 Zhang, W. Z., Shi, F., Hong, H. S., Shang, S. P., and Kirby, J. T.: Tide-surge Interaction Intensified by
 680 the Taiwan Strait, *J. Geophys. Res.-Oceans*, 115, <https://doi.org/10.1029/2009JC005762>,
 681 2010.
 682 Zhang, X., Chu, D., and Zhang, J.: Effects of nonlinear terms and topography in a storm surge model
 683 along the southeastern coast of China: a case study of Typhoon Chan-hom, *Nat. Hazards*, 107,
 684 551-574, <https://doi.org/10.1007/s11069-021-04595-y>, 2021.
 685 Zheng, P., Li, M., Wang, C., Wolf, J., Chen, X., De Dominicis, M., and Hu, Z.: Tide-surge interaction in
 686 the Pearl River Estuary: a case study of Typhoon Hato, *Front. Mar. Sci.*, 7:236,
 687 <https://doi.org/10.3389/fmars.2020.00236>, 2020.